Synthesis and Characterization of Porous Materials from Waste Wheat Bran

Ilknur Demiral |Canan Samdan* |Fatma Betül Kus

Eskişehir Osmangazi University, Faculty of Engineering and Architecture, Department of Chemical Engineering, 26480 Eskişehir, Türkiye.

Corresponding Author
Canan Samdan
E-mail: caydin@ogu.edu.tr Phone: +90222 239 37 50-3664 Fax: +90222 239 36 13
RORID: https://ror.org/01dzjez04

Cite As
Demiral I, et al. Synthesis and Characterization of Porous Materials from Waste Wheat Bran. Hittite J Sci Eng. 2024;11(3):95-104.

CRediT AUTHOR STATEMENT
Ilknur Demiral: Conceptualization, Data curation, Formal Analysis, Investigation, Methodology, Resources, Supervision, Writing – review and editing. **Canan Samdan:** Conceptualization, Data curation, Formal Analysis, Investigation, Methodology, Supervision, Visualization, Writing – original draft & editing. **Fatma Betül Kus:** Conceptualization, Data Curation, Formal Analysis, Methodology, Validation, Writing.

Synthesis and Characterization of Porous Materials from Waste Wheat Bran

Ilknur Demiral | Canan Samdan* | Fatma Betül Kus

Eskişehir Osmangazi University, Faculty of Engineering and Architecture, Department of Chemical Engineering, 26480 Eskişehir, Türkiye.

Abstract

The purpose of this study was to investigate how the amount of $ZnCl_2$ and temperature affect the process of converting waste wheat bran, known for its hemicellulose struc-ture, into porous material. The characterization of the wheat bran was done using proximate and primary component analysis, and Thermogravimetric analysis (TG) test, Fourier Transform Infrared Spectroscopy (FT-IR) spectra, Energy-dispersive X-ray spectroscopy (EDS) results, and Scanning electron microscopy (SEM) images. The influence of temperature on the surface areas of activated carbons is more significant than the impact of varying the amount of $ZnCl_2$. When the carbonization temperature reached 500 °C, porous structures developed, and the highest surface areas achieved for all impregnation ratios (1:1, 2:1, and 3:1) were 1234, 1478, and 1422 m^2/g, respectively. Activated carbon was found to have acidic (0.88 mmol/g) and basic (0.54 mmol/g) functional groups on its surface, after being synthesized through carbonization at 500 °C using $ZnCl_2$ at a 2:1 impregnation ratio in accordance with Boehm titration. This promising activared carbon made from wheat bran, activated by $ZnCl_2$, is efficient and environmentally friendly, and it is a potential solution for water pollution treatment.

Keywords: Activated carbon, surface characterization, biomass (wheat bran), chemical activation, characterization

INTRODUCTION

Activated carbon is a porous material obtained by increasing the carbon content of various materials such as wood, coal, polymer, and biomass at high temperatures through different activation processes. Activated carbons contain hydrogen, nitrogen, sulfur, and oxygen in their internal structure and functional groups attached to their external surfaces. The quality of porous material vary depending on the raw material and synthesis method used (Daoud et al. 2019; Azam et al. 2022). The traditional synthesis of activated carbon consists of two basic steps: carbonization and activation. Carbonization is a process that involves the thermal decomposition of volatile elements from the raw material in an environment without oxygen. This process leads to the removal of components other than carbon and results in the production of materials with a high carbon content. Essentially, cross-links in raw materials are broken down, and the volatile substance content is reduced. During carbonization, the lignocellulosic contents are broken down, which removes elements such as nitrogen, oxygen, and hydrogen (Mahmoud Amer and Ahmed Elwardany 2020).
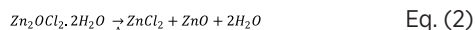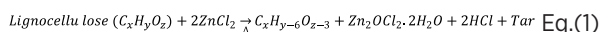
Chemical activation is a process that doesn't involve a different carbonization level. The completely dehydrated sample reacts by coming into contact with dehydrating agents such as NaOH, KOH, $ZnCl_2$ and H_3PO_4 (Reza et al. 2020). Activated carbon with well-developed porous areas can be produced in a single step, reducing the production of volatile matter during pyrolysis and minimizing particle shrinkage and damage to the raw material surface. This results in the production of activated carbon with high efficiency and carbon content (Świątkowski 1999). Biomass and waste materials can be used to produce activated carbon cost-effectively. These materials often have no economic value, and waste disposal poses a problem. Converting them into activated carbon can provide economic value but can also reduce the cost of waste disposal. The use of biomass as a raw material in the production of activated carbon can provide a cheap alternative to commercial activated carbons. Many materials, palm kernels, olive pits, waste sludge and tires, bamboo powder, coconut shells, rice husks and straw, jute fibers, zeolite, sugars, Chinese jujube seeds, wood shavings, tropical trees, palm shells, corn cobs, walnut shells, tobacco stalks, bean pods, hazelnut shells, banana peels, mangosteen shells are used in the production of activated carbon (Rafatullah et al. 2010; Tadda et al. 2016).

Wheat is a crucial crop globally, and its production reached 790198 tonnes in 2022. In Turkey, the 10th largest wheat producer, 15000 tonnes of wheat were planted (FAOSTAT 2024). Wheat bran, a by-product of wheat (approximately 25% by weight), amounts to around 3750 tons per year in Turkey and is a renewable biomass source. It is derived from wheat milling industries and is a readily available natural material, suitable for producing an effective adsorbent. For this reason, wheat bran has been seen as a suitable raw material for the production of activated carbon as an environmentally friendly and renewable resource and was chosen as the carbon source in this study. Zhang and his team utilized wheat bran as a renewable and less enduring source to create carbon electrodes in supercapacitors. According to their research, during the production of carbon via alkali activation, the NaOH/precursor bulk mass was at the 4 state, resulting in durable hexagon pores of carbon from wheat bran with a visible surface area of 2562 m^2/g (Zhang).

Koli et al., prepared activated carbons from wheat bran which were mixed with H_2SO_4 and carried out under a one-step chemical activation under N_2 flow at 773K for 2 h. The maximum Brunauer-Emmett-Teller (BET)surface area was found 757 m^2/g (Koli et al. 2024). Wang et al., reported on wheat bran activated carbon which impregnated with KOH (1:2) as activating agent under nitrogen gas flow rate of 60 cm^3/min in a horizontal tubular furnace at 800 °C for 1 h and had obtained a maximum BET surface area of 2189 m^2/g (Wang et al. 2015). Hu et al., prepared activated carbons from wheat bran by chemical activation with $ZnCl_2$, KOH and $ZnCl_2$-KOH as activating agents in a reactor under argon flow. They report that two-step $ZnCl_2$–KOH activation process was developed to produce wheat bran-derived biocarbon with an high specific surface area of 3200.8 m^2/g (Hu et al. 2024). Around 80% of activated carbons are utilized in liquid-phase applications and are recognized for their excellent performance in eliminating contaminants from different environments (Ioannidou and Zabaniotou 2007; Reza et al. 2020). When $ZnCl_2$ is used, it plays a crucial role as a dehydration agent during activation. Ma's report suggests that the production of ZnO may be explained by the following

equations (1) and (2) (Ma 2017):

$$Lignocellulose\ (C_xH_yO_z) + 2ZnCl_2 \xrightarrow{\Delta} C_xH_{y-6}O_{z-3} + Zn_2OCl_2.2H_2O + 2HCl + Tar \quad Eq.(1)$$

$$Zn_2OCl_2.2H_2O \xrightarrow{\Delta} ZnCl_2 + ZnO + 2H_2O \qquad Eq.\ (2)$$

At elevated temperatures, molten $ZnCl_2$ can facilitate dehydration processes that result in the breakdown of the polymer chains in lignocellulosic biomass, producing H_2O and a carbonaceous phase with thermoplastic properties (Kierzek and Gryglewicz 2020; Zhao et al. 2022). $ZnCl_2$ can then react with H_2O to create $Zn_2OCl_2.2H_2O$. Subsequently, the decomposition of $Zn_2OCl_2.2H_2O$ can generate $ZnCl_2$ vapor. The presence of $ZnCl_2$ vapor and its diffusion can contribute to the development of the final porous carbon structure (Ma et al. 2009; Moralı et al. 2018). Also, $ZnCl_2$ helps to inhibit the production of tar and facilitates the development of a high surface area and porous structure (Demiral and Gündüzoğlu 2010; Zhao et al. 2022). $ZnCl_2$ was chosen as the chemical activation agent in our study. In this study, activated carbons, which have a wide range of usage areas, were produced from wheat bran, which is a large mass of waste. Various properties of the activated carbons produced using various characterization methods, such as surface porosity, were investigated. Activated carbon is a material that is used as an important component in many industries. Our research, which explores the creation of a substance that can generate economic value from leftover wheat bran while also cutting waste disposal expenses, can serve as a valuable model in the literature.

MATERIALS AND METHOD
Devices and Chemicals
The raw material was ground using a Retsch SK-100 mill and then sieved into different particle sizes using an ISO 3310-1 sieve set. For the chemical activation of the raw material, zinc chloride ($ZnCl_2$) obtained from Merck was used. DAIHAN's SMH-6 Model heated magnetic stirrer was used for heating and mixing during the impregnation processes of the raw material. The carbonization process was carried out in a Carbolite TZF 12/75/700 tube furnace. The surface properties of the activated carbons obtained from wheat bran through the chemical activation method, using $ZnCl_2$, were measured by N_2 adsorption. The measurements were performed by changing the relative pressure (P/Po) in the range of 10-6-1 at 77 K, using the Quantchrome Autosorb 1C device. FT-IR analysis of raw materials and activated carbons was carried out on the Perkin Elmer Spectrum device at Eskişehir Osmangazi University Central Research Laboratory Research and Application Center (ARUM). SEM photographs of the raw material were taken at Eskişehir Osmangazi University Central Research Laboratory Research and Application Center (ARUM) with a Hitachi Refulus 8230 FE-SEM brand device. A controlled temperature program (up to 1000 °C at a heating rate of 10 °C/min) was applied to wheat bran in a nitrogen atmosphere using the thermal analysis system (STA-TG/DTA), and the mass change was measured as a function of temperature. The amount of acidic-basic functional group was determined by Boehm titration method of the activated carbon produced at 500 °C at a 2:1 impregnation ratio.

Production of Activated Carbons
Activated carbon was produced using the chemical activation method, wherein $ZnCl_2$ was selected as the chemical agent for impregnation. The impregnation ratios (IRs) of the chemical agent were determined as 1:1, 2:1, and 3:1, after which it was mixed with 20 g of wheat bran and refluxed in a heated magnetic stirrer at 80°C for 6 hours. Once the impregnation process was completed, the sample was filtered, and the water contained in the filtered product was completely removed from the structure by drying it in the oven. To produce activated carbon, wheat bran was treated with $ZnCl_2$ and subjected to simultaneous carbonization and activation processes. 10 g samples that had been impregnated with $ZnCl_2$ were placed in a reactor. The process was carried out for a duration of 1 hour in a vertical tube furnace at temperatures ranging from 400 to 600 °C, starting from laboratory temperature. The carbonization process was carried out in an inert environment, with nitrogen gas flowing at a rate of 100 ml/min. After cooling, the samples were weighed and washed in 0.5 M HCl solution, filtered, and then washed again with boiling distilled water having a pH value of 6-7. Finally, the washed samples were dried in an oven and weighed again. The activated carbons that were created were given names in the format of WB/temperature-/IR.

RESULTS AND DISCUSSION
Characterization of Wheat Bran
Wheat bran was characterized using proximate analysis results, structural components, physical properties, thermogravimetric analysis, FT-IR analysis, elemental analysis and SEM analysis results.

Proximate analysis of wheat bran
The results of moisture, volatile matter, ash, fixed carbon results of wheat bran are given in Table 1. Wheat bran's low ash content of 7.5% makes it a suitable material for producing activated carbon. Ghodrat et al.'s study investigated the in vitro binding capacity of manganese (Mn), zinc (Zn), copper (Cu), and iron (Fe) in wheat and barley. Their proximate analysis findings for wheat bran are similar to our own proximate analysis results. Ghodrat and colleagues found that wheat bran comprises 4.6 wt% ash, 9.55 wt% moisture, and 68.18 wt% volatile matter (Ghodrat et al. 2015). Ghodrat et al. stated that wheat bran can be a suitable source of raw materials for the production of activated carbon. In our study, we thought that wheat bran with wt 7.5% ash content could be a suitable carbon source.

Table 1 Proximate analysis of wheat bran

Proximate Analysis, %	
Moisture	9.6 (ASTM D 4442 – 92)
Ash	7.5 (ASTM D 1102 – 84)
Volatile matter	67.4 (ASTM E 897-82)
Fixed carbon*	15.5

*Bydifference

Results of thermogravimetric analysis of wheat bran
TGA is a thermal analysis technique that observes the mass change of a substance as it is exposed to controlled

temperature and atmospheric environments, either as a function of temperature or time (Escalante, 2022). The TGA graph in Figure 1 shows how organic compounds in wheat bran undergo thermal degradation. In the graph, the primary Y-axis shows the % mass loss observed in the sample based on the applied temperature (green line), the secondary Y-axis shows the differential of the mass loss over time (orange line), and the x-axis shows the temperature applied to the sample.
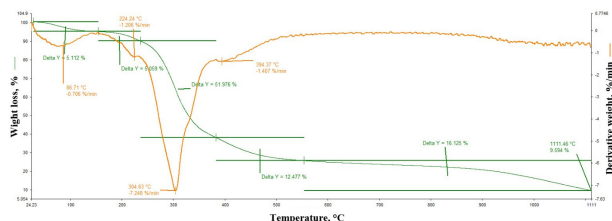

Figure 1 TGA-DTG curve representing the thermal decomposition of wheat bran

The TGA chart of wheat bran showed the first peak at 86.71°C, with a weight loss of 5.11%. This could be due to the evaporation of water present in the bran. The next weight loss occurred at 224.24°C, with a weight loss of 5.05%. This is because the hemicellulose present in bran begins to decompose at this temperature. According to a study by Li et al. (2021), the hemicellulose in the structure of wheat bran decomposes at 299°C. At 304.63°C, the wheat bran TGA plot shows a faster weight loss (51.97%) (Li et al. 2021). It is believed that this weight loss is due to the continued decomposition of hemicellulose, as well as the decomposition of cellulose. Cellulose decomposes at higher temperatures and is slower than hemicellulose. It can be inferred that the mass loss that continues from 394°C until 1111°C is due to the lignin present in the bran (Escalante et al. 2022). The TGA curve of wheat bran, which was studied by Pooladi et al., exhibits very similar characteristics to the TGA curve we acquired in our own research. Pooladi and colleagues noted in their research that the decomposition of wheat bran occurs in three distinct stages at temperature intervals of 50-180 °C, 200-800 °C, and 800-1000 °C like our study results (Pooladi et al. 2021) the uptake process of methylene blue (MB)

FT-IR analysis results of wheat bran

Infrared spectroscopy (IR) is a technique that relies on the vibrations of atoms in the chemical composition of materials. With FT-IR, researchers can detect the presence of many functional groups in commonly used materials such as adsorbents. For example, an adsorbent such as activated carbon may contain various functional groups such as carboxylic acids, quinones, phenolic groups, lactones, ketones, ethers, pyridine-like groups, amides, and amines (Kabdaşlı et al. 2009; Shafeeyan et al. 2010; Pellenz et al. 2023)application of electrocoagulation using common electrode materials (aluminum and stainless steel. The FT-IR image of wheat bran is shown in Figure 2.
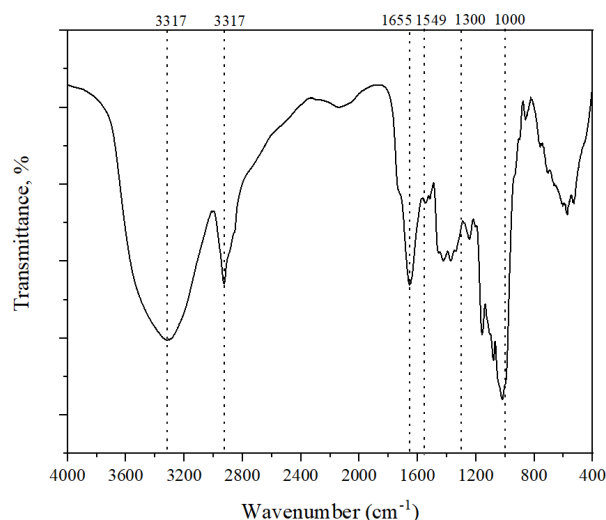

Figure 2 FT-IR image of wheat bran

FT-IR spectroscopy provides detailed information about the chemical bonds of organic components in wheat bran. According to the analysis results, hydroxyl groups, methyl and methylene groups, carboxylic acid groups, aldehyde or ketone groups, aromatic ring vibrations, vibrations of hydroxyl groups of cellulose, vibrations of glycosidic bonds of cellulose were detected in the bran. The band at 3317 cm^{-1} indicates the presence of hydroxyl (-OH) groups (Fanning and Vannice 1993; Shafeeyan et al. 2011; Hoseinzadeh Hesas et al. 2013). The peak at 2924 cm^{-1} indicates the presence of methyl (-CH3) and methylene (-CH2-) groups (Shen et al. 2010; Kaouah et al. 2013) The peak at 1736 cm^{-1} indicates the presence of carboxylic acid (-C=O) groups (Jia et al. 2001; Gulnaz et al. 2006; Biniak et al. 2013; Barroso-Bogeat et al. 2014). The peak at 1655 cm^{-1} indicates the presence of aldehyde (R-CHO) or ketone (R-CO-R') (Cagniant et al. 1998; Boonamnuayvitaya et al. 2005; El-Hendawy 2006). The peak at 1549 cm^{-1} indicates the presence of aromatic ring (-C=C-) vibrations (Guo and Rockstraw 2007; Momcilovic et al. 2011). The peaks at 1000-1300 cm^{-1} are assigned to C=O stretching in acids, alcohols, phenols, ethers, and esters (Gurten et al. 2012; Xu et al. 2014). In a study by Silva et al., Fourier transform infrared (FTIR) analysis of wheat bran was performed. Similar to the results in our study, their analysis identified specific bond structures indicating the presence of aromatic and organic compounds such as hemicellulose and cellulose in wheat bran (Silva et al. 2022).

Results of elemental analysis of wheat bran

Table 2 shows the EDS analysis results of wheat bran. Based on these data, it appears that wheat bran has a high carbon content. The presence of nitrogen indicates that wheat bran contains nitrogenous compounds such as proteins, amino acids, and other organic compounds (Chaquilla-Quilca et al. 2016). A high percentage of oxygen indicates that wheat bran contains largely carbohydrates, oxygenated organic compounds such as cellulose and lignin (Chaquilla-Quilca et al. 2016).

Table 2 EDS analysis results of wheat bran

%C	%N	%O
52,61	3,79	43,59

SEM image of wheat bran

The SEM image of wheat bran is given in Figure 3. According to the images taken with the SEM device, raw wheat bran, which has not been subjected to any chemical/physical effects, has a non-porous structure (Figure 3). This shows that the raw material has a very small surface area before activation and carbonization.
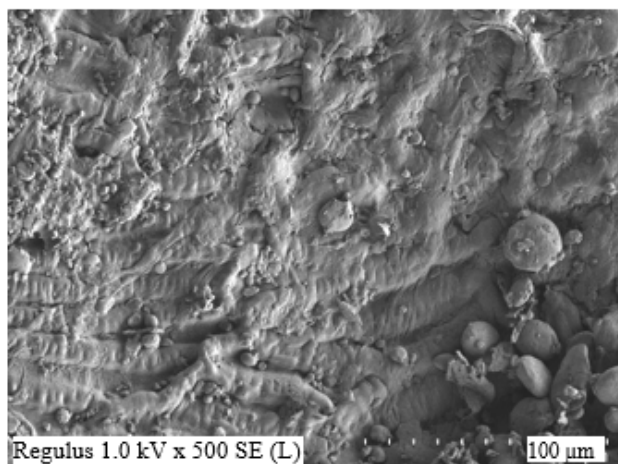
Figure 3 SEM image of wheat bran

Activated Carbon Characterisation

The physical properties of activated carbons produced from wheat bran with $ZnCl_2$ at different IRs by mass and at different carbonization temperatures are given under this heading.

Physical properties of activated carbon

The properties of the surface pores of activated carbon vary depending on the ratio of chemicals used in the production process to the raw material and the temperature at which carbonization is carried out. This process reveals the carbonaceous structure and removes volatile components from it. We synthesized activated carbons under various conditions and have provided the properties of their porous

structures in Table 3.

When the surface areas of the samples are compared according to the carbonization temperatures after chemical impregnation at 1:1, 2:1 and 3:1 $ZnCl_2$/raw material ratios, it shows that the carbonization process at 500 °C is effective in increasing the surface area. In all IRs, micropore volumes first increased from 400 °C to 500 °C and then were adversely affected by the temperature increase. As the temperature increased from 400 °C to 600 °C in 1:1 and 2:1 IRs, the V_{mic}/V_{tot} ratio changed in direct proportion to the temperature increase, while the V_{mez}/V_{tot} ratio was adversely affected. Mean pore diameters contracted from 33.05 Å to 23.40 Å for 1:1 and from 28.23 Å to 22.92 Å for 2:1 IRs, respectively. In the 3:1 IR, the opposite results were encountered. When the chemical impregnation process was carried out with a $ZnCl_2$/raw material ratio of 3, the increase in the temperature at which carbonization took place (400 °C-600 °C) caused changes in the micro and meso pore ratios. The change in temperature caused V_{mic}/V_{tot} to change from 0.57 to 0.48 and V_{mez}/V_{tot} to change from 0.43 to 0.52. With the increasing temperature at the high impregnation ratio, the micropores expanded and turned into meso pores.

When the surface areas covered by the porous structures of the synthesized carbon-structured materials are compared to the IR at 500 °C, the highest surface area and pore volume were obtained as 1487 m²/g and 1.17 cm³/g respectively at a 2:1 IR. As the amount of $ZnCl_2$ used in activation increased at all temperatures, both micro and mesopores first increased for IR 1:1 to 2:1 and then were adversely affected when the IR increased from 2:1 to 3:1. Similar to our study findings, Zhang et al. discovered that excessive chemical use leads to the degradation of pore structures. They observed that the activated carbons they produced from wheat bran with NaOH displayed underdeveloped pore structures at a low impregnation rate (IR; 3:1). Furthermore, they noted that the pores were damaged when they employed high amounts of alkali (IR: 5/:1) (Zhang et al. 2019).

These results highlight the effect of impregnation ratio and temperature parameters on surface properties in the synthesis of porous carbonaceous structures. It was concluded that the study in the production of activated carbon by $ZnCl_2$ activation from wheat bran at 600 °C and at an IR of 3:1 adversely affects the surface area. It has been determined that the highest surface area can be achieved with activated

Table 3 Pore properties of carbonaceous structures synthesized under various conditions.

ID	S_{BET} (m²/g)	V_{mic} (cm³/g)	V_{mez} (cm³/g)	V_{tot} (cm³/g)	V_{mic}/V_{tot}	V_{mez}/V_{tot}	D_p (Å)
WB/400/1	427	0.163	0.189	0.352	0.46	0.54	33.05
WB/500/1	**1234**	0.477	0.257	0.734	0.65	0.35	23.75
WB/600/1	1056	0.425	0.216	0.641	0.66	0.34	23.4
WB/400/2	685	0.251	0.233	0.484	0.52	0.48	28.23
WB/500/2	**1487**	0.538	0.632	1.17	0.46	0.54	23.54
WB/600/2	1439	0.526	0.298	0.824	0.64	0.36	22.92
WB/400/3	681	0.251	0.188	0.439	0.57	0.43	25.81
WB/500/3	**1422**	0.493	0.396	0.889	0.55	0.45	33.07
WB/600/3	1369	0.476	0.521	0.997	0.48	0.52	29.13

carbon production at 500 °C IR of 2:1. Examples of surface areas of activated carbons produced from various sources are given in Table 4.

Table 4 Production methods and surface areas of activated carbons produced from various biomass sources.

Raw materials	Activation Method	Surface Area	Reference
Wheat Bran	NaOH /Chemical activation	2543 m^2/g	(Zhang et al. 2004)
Date Palm	H_3PO_4 / Chemical activation	1283 m^2/g	(Daoud et al. 2019) they applied to eliminate a commercial reactive dye BEZAKTIV Red S-Max (BRSM
Jujube beans	H_3PO_4 / Chemical activation	1896 m^2/g	
Barley stalk	CO_2 / Physical activation	789 m^2/g	(Pallares et al. 2018)
Barley stalk	Steam / Physical activation	553 m^2/g	
Cherry stone	$ZnC2I_2$ / Chemical activation	1704 m^2/g	(Angin 2014)
Wheat Bran	$ZnCl_2$ / Chemical activation	1487 m^2/g	ın this study

Volumetric changes of N_2 gas adsorbed on the surface of synthesized porous materials with relative pressure
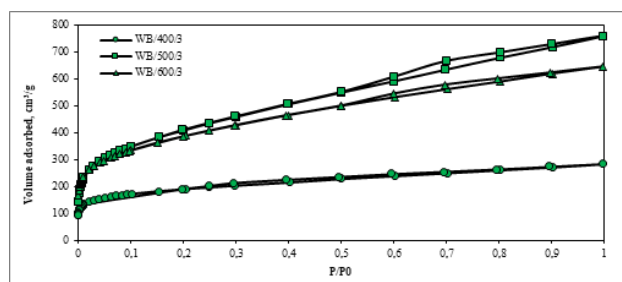
Adsorption-desorption isotherm are graphs that show the relationship between the relative pressure applied at constant temperature and the amount of gas adsorbed or desorbed. Classified by the International Union of Pure and Applied Chemistry (IUPAC), these isotherms are divided into six different categories. Figure 4 presents the N_2 adsorption-desorption isotherm graphs of porous materials synthesized at three different temperatures when impregnation was made using chemicals with the $ZnCl_2$/raw material ratio of 1:1, 2:1 and 3:1 in the chemical activation stage.
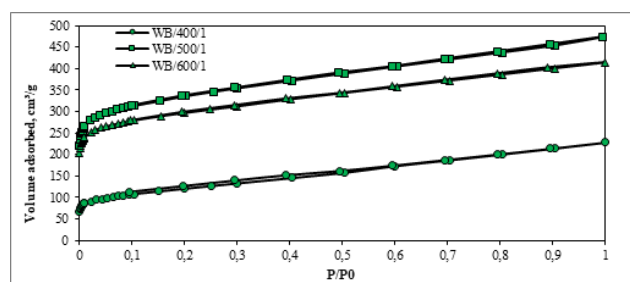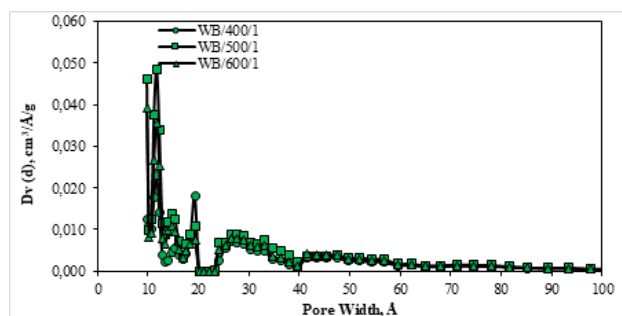

(a)
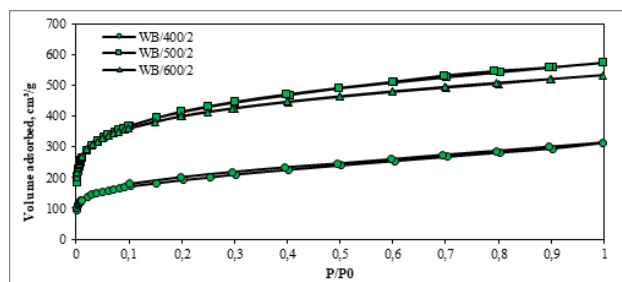
(b)

(c)

Figure 4 N_2 adsorption-desorption isotherm graphs of porous materials synthesized at three different temperatures at (a) 1:1 IR, (b) 2:1 IR, and (c) 3:1 IR.

As shown in Figure 4 (a) and (b), our activated carbon samples have been rigorously tested and found to comply with Type I isotherms as classified by IUPAC. This confirms that the pore structures of our product have more micro-sized pore diameters. Type I isotherms exhibit a rapid rise at low pressures, which then slows down as saturation is reached (Leong et al. 2019). The WB/400/3 conformed to Type I isotherms, while the WB/500/3 and WB/600/3 samples conformed to Type I and Type IV isotherms (Figure 4 (c)). Type IV isotherms are characterized by hysteresis resulting from intrapore condensations at high relative pressures. They are commonly found in porous materials with narrow-mouth pore structures containing mesopores (Meng et al. 2019).

Pore size distributions of synthesized porous materials
The pore structures of various adsorbents may vary in different widths, lengths and diameters. Figure 5 shows the diversity of pore sizes for each sample.
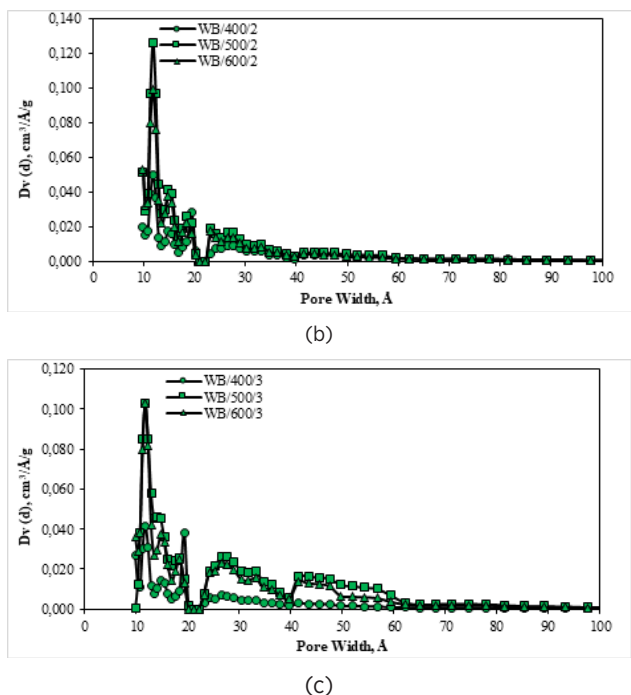

(a)

(b)

(c)

Figure 5 Pore size distributions of porous materials synthesized at three different temperatures at (a) 1:1 IR, (b) 2:1 IR, and (c) 3:1 IR

Figure 5 shows the pore size distributions of activated carbons produced at different IRs and carbonization temperatures. As a result of the examination, it is seen that the vast majority of these activated carbons have micropores between 10-20 Å (1-2 nm). However, meso pore peaks between 20-60 Å were also detected in some samples.

Acidic groups and basic groups amounts of synthesized porous materials determined by Boehm method

Among the activated carbons produced in this study, the highest surface area was obtained in WB/500/2. Acidic groups and basic groups amounts of WB/500/2 is given in Table 5.

Table 5 Acidic groups and basic groups amounts of WB/500/2.

Total acidic group (mmol/g)	Total basic group (mmol/g)	Lactonic (mmol/g)	Phenolic (mmol/g)	Carboxyllic (mmol/g)
0.88	0.54	0.1	0.44	0.3

Boehm titration is a widely used method for determining the organic structural functionality of carbonaceous materials. This method separates various surface functional groups from each other using NaOH, Na_2CO_3, and $NaHCO_3$ compounds. $NaHCO_3$ detects carboxylic groups, Na_2CO_3 detects lactonic groups, and NaOH detects phenolic groups. The method is very effective in determining the functional groups in the structure, especially in adsorption studies (Liu et al. 2018). The total acidity and alkalinity values of the WB/500/2 sample were determined to be 0.88 and 0.54 mml/g, respectively. It can be said that the sample contains lactonic, phenolic, and carboxylic groups on its surface. Activated carbon has an amphoteric structure with both acidic and basic functional groups on its surface.
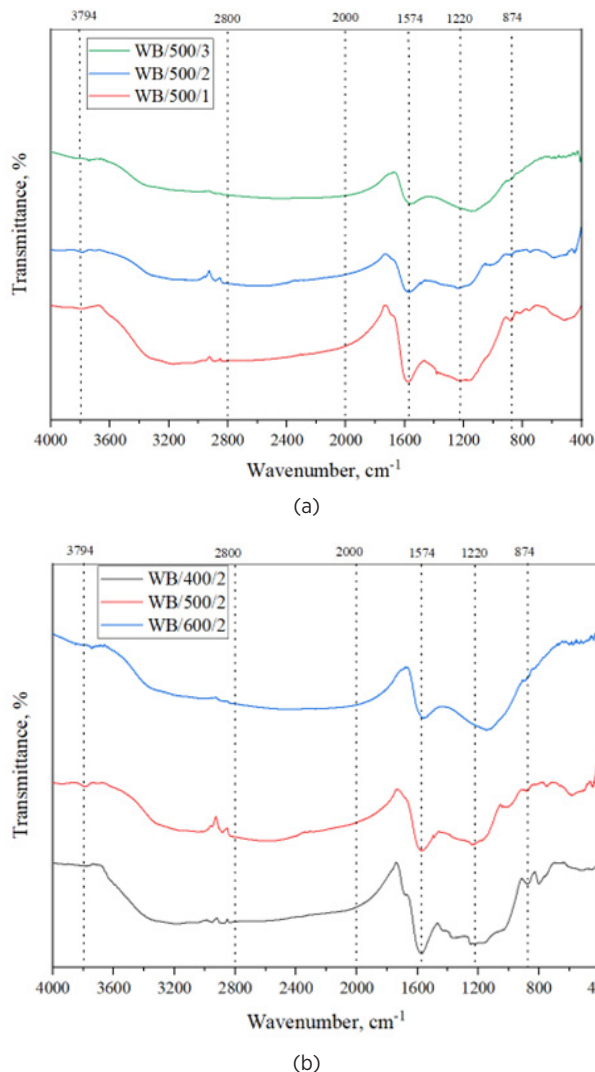
FT-IR analysis results of synthesized porous materials

(a)

(b)

Figure 6 (a) shows FT-IR images of samples WB/500/1, WB/500/2 and WB/500/3 while Figure 6 (b) displays FT-IR images of samples WB/400/2, WB/500/2 and WB/600/2.

The IR spectra seen in Figure 6 shows peaks at 2885, 1574, 1220, 1157 and 874, 816 cm^{-1}. The peak at 3794 cm^{-1} in the spectra of WB/500/2 and WB/600/2 may indicate the presence of hydroxyl (-OH) groups (Fanning and Vannice 1993; Shafeeyan et al. 2011; Hoseinzadeh Hesas et al. 2013). The peaks seen between 2800-2000 cm^{-1} are generally attributed to $\upsilon(C\equiv C)$ vibration in alkyne groups and $\upsilon(C-H)$ bond vibrations in aldehydes (Boonamnuayvitaya et al. 2005; Deng et al. 2009; Hoseinzadeh Hesas et al. 2013). The broad band seen at 1574 cm^{-1} indicates the presence of υ (C=C) bonds in aromatic functional groups (Baccar et al. 2009; Kaouah et al. 2013). This indicates that there are aromatic components in the structure of activated carbon. The band at 1220 cm^{-1} may indicate the presence of $\upsilon(C-O)$ bonds (Guo and Rockstraw 2007; Liu et al. 2010). The peak at 874 cm^{-1} may indicate the presence of C-Cl

bonds. In the structure of this activated carbon, chlorinated components from $ZnCl_2$ can be found (Mahapatra et al. 2012).

Elemental analysis results of synthesized porous materials

The elemental analysis results of the samples WB/500/1, WB/500/2 and WB/500/3 are given in Table 6. According to the results, when the IR value increased from 1:1 to 2:1 at 500 °C, the carbon composition of the activated carbon first increased slightly. When the IR value increased to 3:1, the carbon amount decreased. This indicates that large amounts of $ZnCl^2$ result in a lower carbon yield. Moreover, as the impregnation ratio increased, there was a decrease in the nitrogen composition and an increase in the oxygen composition. This suggests that on the synthesized porous materials, the number of N-containing functional groups decreased while oxygen-containing groups increased.

Table 6 The elemental analysis results of the samples WB/500/1, WB/500/2 and WB/500/3.

|	%C	%N	%O
WB/500/1	86.43	5.76	6.93
WB/500/2	88.41	4.17	6.89
WB/500/3	73.21	0.67	26.12

SEM (Scanning Electron Microscope) images of synthesized porous materials

The SEM images of the WB/400/2, WB/500/2 and WB/600/2 examples are given Figure 7. From Figure 7, the change in the pore structure of the activated carbon according to the production temperature can be seen in the 2:1 IR. When the images are examined, it can be seen that the pores of the WB/400/2 sample have started to form, the WB/500/2 sample has more prominent and larger pores, and the WB/600/2 has a less porous structure.

These results show that production temperature conditions have a significant effect on the pore structure of activated carbon. Activated carbons produced at 500 °C tend to have larger and more prominent pores. However, when the temperature is raised to 600 °C, the structure of the pores can be disrupted and adversely affect the surface area of the activated carbon.
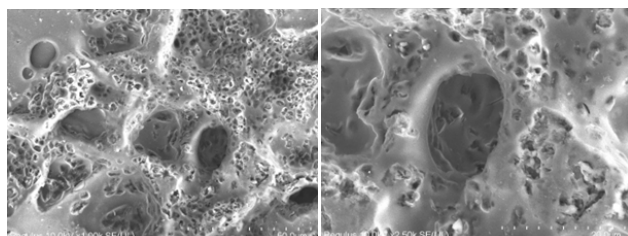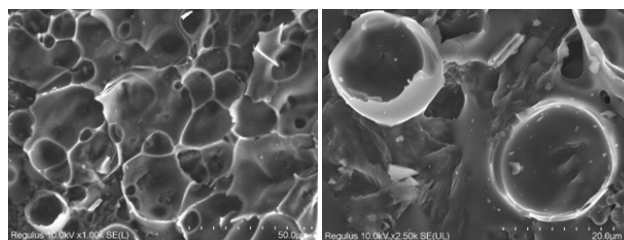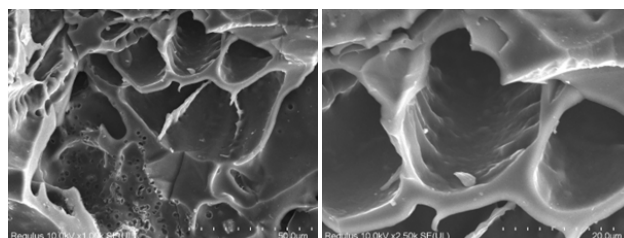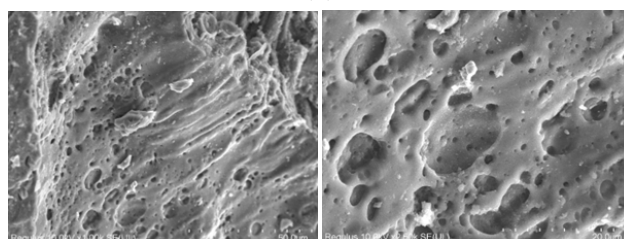

(a)
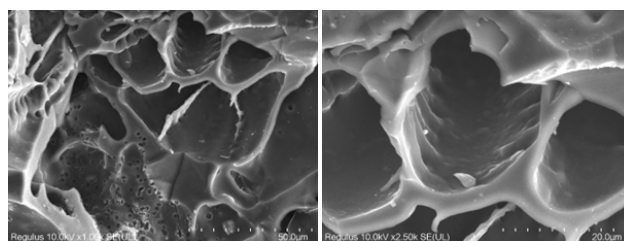
(b)
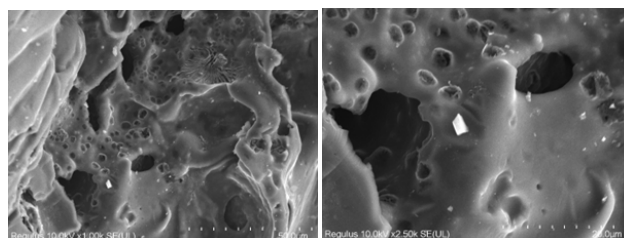
(c)

Figure 7 SEM images of synthesized porous materials at 1000 and 25000 magnifications, (a) WB/400/2, (b) WB/500/2 and, (c) WB/600/2

(a)

(b)

(c)

Figure 8 SEM images of synthesized porous materials at 1000 and 25000 magnifications, (a) WB/500/1, (b) WB/500/2 and, (c) WB/500/3

The SEM images presented in Figure 8 illustrate the impact of the impregnation ratio on the pore structure of synthesized porous materials during its production process. Synthesized

porous material with a 1:1 $ZnCl_2$/raw material has very small and densely packed pores, while synthesized porous material with a 2:1 $ZnCl_2$/raw material has wider and less dense pores. However, the synthesized porous material with a 3:1 $ZnCl_2$/raw material has a less porous structure as the very high impregnation ratio has closed the pores.

CONCLUSION

In this study, activated carbon was produced from wheat bran by the chemical activation method. WB has low ash content (7.05%), carbon (52.61%) and oxygen (43.59%). The increase in the amount of chloride salt used in the chemical activation phase caused a decrease in the carbon content of active carbons and an increase in the oxygen content. The influence of temperature on the surface areas of activated carbons is more significant than the impact of varying the amount of $ZnCl_2$. When the surface areas of the samples were compared according to the carbonization temperatures after the chemical impregnation process performed at $ZnCl_2$/raw material ratios as 1:1, 2:1 and 3:1, the highest surface area was obtained at 500 °C as 1234, 1478, and 1422 m^2/g, respectively. The highest surface area was obtained as 1487 m^2/g in the WB/500/2 sample. The temperature increases in 1:1 and 2:1 impregnation ratio (from 400 °C to 600 °C) led to a decrease in the average pore diameters of the activated carbons.

Acknowledgment

References

1. Daoud M, Benturki O, Girods P, Donnot A, Fontana S. Adsorption ability of activated carbons from Phoenix dactylifera rachis and Ziziphus jujube stones for the removal of commercial dye and the treatment of dyestuff wastewater. Microchem J. 2019 Jul;148:493–502.

2. Azam K, Shezad N, Shafiq I, Akhter P, Akhtar F, Jamil F, et al. A review on activated carbon modifications for the treatment of wastewater containing anionic dyes. Chemosphere. 2022 Nov 1;306:135566.

3. Mahmoud Amer, Ahmed Elwardany. Biomass Carbonization. In: Mansour Al Qubeissi, Ahmad El-kharouf, Hakan Serhad Soyhan, editors. Renewable Energy [Internet]. Rijeka: IntechOpen; 2020 [cited 2024 May 25]. p. Ch. 11. Available from: https://doi.org/10.5772/intechopen.90480

4. Reza MS, Yun CS, Afroze S, Radenahmad N, Bakar MSA, Saidur R, et al. Preparation of activated carbon from biomass and its' applications in water and gas purification, a review. Arab J Basic Appl Sci. 2020 Jan 1;27(1):208–38.

5. Świątkowski A. Industrial carbon adsorbents. In: Adsorption and its Applications in Industry and Environmental Protection. 1999. (Studies in Surface Science and Catalysis; vol. 179).

6. Rafatullah Mohd, Sulaiman O, Hashim R, Ahmad A. Adsorption of methylene blue on low-cost adsorbents: A review. J Hazard Mater. 2010 May;177(1–3):70–80.

7. Tadda MA, Ahsan A, Shitu A, ElSergany M, Arunkumar T, Jose B, et al. A review on activated carbon: process, application and prospects. J Adv Civ Eng Pract Res. 2016;2(1):7–13.

8. FAOSTAT. Value of Agricultural Production [Internet]. 2024. Available from: https://www.fao.org/faostat/en/#data/QV

9. Zhang Y. Preparation of Hierarchical Porous Carbon from Wheat Bran for Free-Standing Electrode of High Areal Capacitance Supercapacitor.

10. Koli A, Kumar A, Pattanshetti A, Supale A, Garadkar K, Shen J, et al. Hierarchical Porous Activated Carbon from Wheat Bran Agro-Waste: Applications in Carbon Dioxide Capture, Dye Removal, Oxygen and Hydrogen Evolution Reactions. ChemPlusChem. 2024 Mar;89(3):e202300373.

11. Wang D, Min Y, Yu Y. Facile synthesis of wheat bran-derived honeycomb-like hierarchical carbon for advanced symmetric supercapacitor applications. J Solid State Electrochem. 2015 Feb;19(2):577–84.

12. Hu X, Li Y, Du J, Sun J, He C, Xiong Y, et al. Waste Biomass-Derived Carbon with Ultrahigh Adsorption Capacity for Anionic and Cationic Dyes and Antibiotics in a Wide pH Range. Ind Eng Chem Res. 2024 Mar 13;63(10):4702–13.

13. Ioannidou O, Zabaniotou A. Agricultural residues as precursors for activated carbon production—A review. Renew Sustain Energy Rev. 2007 Dec;11(9):1966–2005.

14. Ma Y. Comparison of Activated Carbons Prepared from Wheat Straw via ZnCl2 and KOH Activation. Waste Biomass Valorization. 2017 Apr;8(3):549–59.

15. Kierzek K, Gryglewicz G. Activated Carbons and Their Evaluation in Electric Double Layer Capacitors. Molecules. 2020 Sep 16;25(18):4255.

16. Zhao H, Zhong H, Jiang Y, Li H, Tang P, Li D, et al. Porous ZnCl2-Activated Carbon from Shaddock Peel: Methylene Blue Adsorption Behavior. Materials. 2022 Jan 25;15(3):895.

17. Ma J, Yang H, Li L, Xie X, Liu B, Zhang L. Synthesis of Aligned ZnO Submicron Rod Arrays by Heating Zinc Foil Covered with ZnCl2 Solution. Acta Chim Sin. 2009 Jul 14;67:1515–22.

18. Moralı U, Demiral H, Şensöz S. Optimization of activated carbon production from sunflower seed extracted meal: Taguchi design of experiment approach and analysis of variance. J Clean Prod. 2018 Jul;189:602–11.

19. Demiral H, Gündüzoğlu G. Removal of nitrate from aqueous solutions by activated carbon prepared from sugar beet bagasse. Bioresour Technol. 2010 Mar;101(6):1675–80.

20. Ghodrat A, Yaghobfar A, Ebrahimnezhad Y, Aghdam Shahryar H, Gorbani A. In vitro Binding Capacity of Wheat and Barley for Mn, Zn, Cu and Fe. Int J Life Sci. 2015 Sep 26;9:56.

21. Li C, Wang L, Chen Z, Li Y, Luo X, Zhao F. Ozonolysis of wheat bran in subcritical water for enzymatic saccharification and polysaccharide recovery. J Supercrit Fluids. 2021 Feb;168:105092.

22. Escalante J, Chen WH, Tabatabaei M, Hoang AT, Kwon EE, Andrew Lin KY, et al. Pyrolysis of lignocellulosic, algal, plastic, and other biomass wastes for biofuel production and circular bioeconomy: A review of thermogravimetric analysis (TGA) approach. Renew Sustain Energy Rev. 2022 Nov;169:112914.

23. Pooladi H, Foroutan R, Esmaeili H. Synthesis of wheat bran sawdust/Fe3O4 composite for the removal of methylene blue and methyl violet. Environ Monit Assess. 2021 Apr 16;193(5):276.

24. Kabdaşlı I, Vardar B, Arslan-Alaton I, Tünay O. Effect of dye auxiliaries on color and COD removal from simulated reactive dyebath effluent by electrocoagulation. Chem Eng J. 2009 May;148(1):89–96.

25. Shafeeyan MS, Daud WMAW, Houshmand A, Shamiri A. A review on surface modification of activated carbon for carbon dioxide adsorption. J Anal Appl Pyrolysis. 2010 Nov;89(2):143–51.

26. Pellenz L, De Oliveira CRS, Da Silva Júnior AH, Da Silva LJS, Da Silva L, Ulson De Souza AA, et al. A comprehensive guide for characterization of adsorbent materials. Sep Purif Technol. 2023 Jan;305:122435.

27. Fanning PE, Vannice MA. A DRIFTS study of the formation of surface groups on carbon by oxidation. Carbon. 1993;31(5):721–30.

28. Shafeeyan MS, Daud WMAW, Houshmand A, Arami-Niya A. Ammonia modification of activated carbon to enhance carbon dioxide adsorption: Effect of pre-oxidation. Appl Surf Sci. 2011 Feb;257(9):3936–42.

29. Hoseinzadeh Hesas R, Arami-Niya A, Wan Daud WMA, Sahu JN. Preparation and Characterization of Activated Carbon from Apple Waste by Microwave-Assisted Phosphoric Acid Activation: Application in Methylene Blue Adsorption. BioResources. 2013 Apr 30;8(2):2950–66.

30. Shen DK, Gu S, Bridgwater AV. Study on the pyrolytic behaviour of xylan-based hemicellulose using TG–FTIR and Py–GC–FTIR. J Anal Appl Pyrolysis. 2010 Mar;87(2):199–206.

31. Kaouah F, Boumaza S, Berrama T, Trari M, Bendjama Z. Preparation and characterization of activated carbon from wild olive cores (oleaster) by H3PO4 for the removal of Basic Red 46. J Clean Prod. 2013 Sep;54:296–306.

32. Jia Y, Xiao B, Thomas K. Adsorption of metal ions on nitrogen surface functional groups in activated carbons. Langmuir. 2001 Dec;18.

33. Gulnaz O, Kaya A, Dincer S. The reuse of dried activated sludge for adsorption of reactive dye. J Hazard Mater. 2006 Jun;134(1–3):190–6.

34. Biniak S, Świątkowski A, Pakuła M, Sankowska M, Kuśmierek K, Trykowski G. Cyclic voltammetric and FTIR studies of powdered carbon electrodes in the electrosorption of 4-chlorophenols from aqueous electrolytes. Carbon. 2013 Jan;51:301–12.

35. Barroso-Bogeat A, Alexandre-Franco M, Fernandez-Gonzalez C, Gomez-Serrano V. FT-IR Analysis of Pyrone and Chromene Structures in Activated Carbon. Energy Fuels. 2014 Jun;28(6):4096–103.

36. Cagniant D, Gruber R, Boudou JP, Bilem C, Bimer J, Salbut PD. Structural Characterization of Nitrogen-Enriched Coals. Energy Fuels. 1998 Jul 1;12(4):672–81.

37. Boonamnuayvitaya V, Sae-ung S, Tanthapanichakoon W. Preparation of activated carbons from coffee residue for the adsorption of formaldehyde. Sep Purif Technol. 2005 Mar;42(2):159–68.

38. El-Hendawy ANA. Variation in the FTIR spectra of a biomass under impregnation, carbonization and oxidation conditions. J Anal Appl Pyrolysis. 2006 Mar;75(2):159–66.

39. Guo Y, Rockstraw DA. Activated carbons prepared from rice hull by one-step phosphoric acid activation. Microporous Mesoporous Mater. 2007 Mar;100(1–3):12–9.

40. Momcilovic M, Purenovic M, Bojic A, Zarubica A, Randelovic M. Removal of lead(II) ions from aqueous solutions by adsorption onto pine cone activated carbon. Desalination. 2011 Aug;276(1–3):53–9.

41. Gurten II, Ozmak M, Yagmur E, Aktas Z. Preparation and characterisation of activated carbon from waste tea using K2CO3. Biomass Bioenergy. 2012 Feb;37:73–81.

42. Xu J, Chen L, Qu H, Jiao Y, Xie J, Xing G. Preparation and characterization of activated carbon from reedy grass leaves by chemical activation with H3PO4. Appl Surf Sci. 2014 Nov;320:674–80.

43. Silva TP, Ferreira AN, De Albuquerque FS, De Almeida Barros AC, Da Luz JMR, Gomes FS, et al. Box–Behnken experimental design for the optimization of enzymatic saccharification of wheat bran. Biomass Convers Biorefinery. 2022 Dec;12(12):5597–604.

44. Chaquilla-Quilca G, Balandrán-Quintana RR, Azamar-Barrios JA, Ramos-Clamont Montfort G, Mendoza-Wilson AM, Mercado-Ruiz JN, et al. Synthesis of tubular nanostructures from wheat bran albumins during proteolysis with V8 protease in the presence of calcium ions. Food Chem. 2016 Jun;200:16–23.

45. Zhang Y, Song X, Xu Y, Shen H, Kong X, Xu H. Utilization of wheat bran for producing activated carbon with high specific surface area via NaOH activation using industrial furnace. J Clean Prod. 2019 Feb;210:366–75.

46. Zhang T, Walawender W, Fan L, Fan M, Daugaard D, Brown R. Preparation of activated carbon from forest and agricultural residues through CO activation. Chem Eng J. 2004 Dec 15;105(1–2):53–9.

47. Pallares J, González-Cencerrado A, Arauzo I. Production and characterization of activated carbon from barley straw by physical activation with carbon dioxide and steam. Biomass Bioenergy. 2018 Aug;115:64–73.

48. Angin D. Production and characterization of activated carbon from sour cherry stones by zinc chloride. Fuel. 2014 Jan;115:804–11.

49. Leong ZY, Lu G, Yang HY. Three-dimensional graphene oxide and polyvinyl alcohol composites as structured activated carbons for capacitive desalination. Desalination. 2019 Feb;451:172–81.

50. Meng H shan, Chen C, Yan Z run, Li X yan, Xu J, Sheng G ping. Co-doping polymethyl methacrylate and copper tailings to improve the performances of sludge-derived particle electrode. Water Res. 2019 Nov;165:115016.

51. Liu Z, Zhao C, Wang P, Zheng H, Sun Y, Dionysiou DD. Removal of carbamazepine in water by electro-activated carbon fiber-peroxydisulfate: Comparison, optimization, recycle, and mechanism study. Chem Eng J. 2018 Jul;343:28–36.

52. Deng H, Yang L, Tao G, Dai J. Preparation and characterization of activated carbon from cotton stalk by microwave assisted chemical activation—Application in methylene blue adsorption from aqueous solution. J Hazard Mater. 2009 Jul 30;166(2–3):1514–21.

53. Baccar R, Bouzid J, Feki M, Montiel A. Preparation of activated carbon from Tunisian olive-waste cakes and its application for adsorption of heavy metal ions. J Hazard Mater. 2009 Mar;162(2–3):1522–9.

54. Liu QS, Zheng T, Wang P, Guo L. Preparation and characterization of activated carbon from bamboo by microwave-induced phosphoric acid activation. Ind Crops Prod. 2010 Mar;31(2):233–8.

55. Mahapatra K, Ramteke DS, Paliwal LJ. Production of activated carbon from sludge of food processing industry under controlled pyrolysis and its application for methylene blue removal. J Anal Appl Pyrolysis. 2012 May;95:79–86.